POLITECNICO DI TORINO
Repository ISTITUZIONALE

Video-based diagnosis of a rolling element bearing using a high-speed camera: Feedback on the Survishno 2023 conference contest

Original
Video-based diagnosis of a rolling element bearing using a high-speed camera: Feedback on the Survishno 2023 conference contest / Leclère, Q., André, H., Antoni, J., Burel, A., Capdessus, C., Cocconcelli, M., D'Elia, G., Daga, A.P., Dion, J., El Badaoui, M., El Hidali, A., Garibaldi, L., Girardin, F., Griffaton, J., Gryllias, K., Han, Y., Helsen, J., Karkafi, F., Kestel, K., Kordylas, L., et al.. - In: MECHANICAL SYSTEMS AND SIGNAL PROCESSING. - ISSN 0888-3270. - ELETTRONICO. - 230:(2025), pp. 1-16. [10.1016/j.ymssp.2025.112601]

Availability:
This version is available at: 11583/2998821 since: 2025-04-03T13:26:55Z

Publisher:
Elsevier

Published
DOI:10.1016/j.ymssp.2025.112601

Terms of use:

This article is made available under terms and conditions as specified in the corresponding bibliographic description in the repository

Publisher copyright

(Article begins on next page)

19 November 2026

Mechanical Systems and Signal Processing 230 (2025) 112601

Contents lists available at ScienceDirect

Mechanical Systems and Signal Processing

journal homepage: www.elsevier.com/locate/ymssp

Video-based diagnosis of a rolling element bearing using a high-speed camera: Feedback on the Survishno 2023 conference contest

Quentin Leclère [a,*], Hugo André [b], Jérôme Antoni [a], Arthur Burel [c,q], Cécile Capdessus [j], Marco Cocconcelli [i], Gianluca D'Elia [i], Alessandro Paolo Daga [d], Jean-Luc Dion [o], Mohammed El Badaoui [m,b], Abdallah El Hidali [l], Luigi Garibaldi [d], François Girardin [a], Julien Griffaton [l], Konstantinos Gryllias [e,f], Yunhyeok Han [o], Jan Helsen [h,p], Fadi Karkafi [m,a], Kayacan Kestel [h], Layla Kordylas [o], Deepti Kunte [e,g], Stefania Lo Feudo [o], Adrien Marsick [a], Douw Marx [e,f], Alex Ricardo Mauricio [e,f], Johann Miranda-Fuentes [n], Cédric Peeters [h,p], Thomas Poupon [k], Didier Rémond [c], Franck Renaud [o], Julien Roussel [j], Jimmy Touzet [b], Toby Verwimp [e,f], Luca Viale [d], Mahsa Yazdanianasr [e,f], Rui Zhu [e,f]

[a] INSA Lyon, LVA, UR, 69621 Villeurbanne, France
[b] Université Jean Monnet Saint-Etienne, IUT de Roanne, LASPI, UR, F-42300, Roanne, France
[c] INSA Lyon, CNRS, LaMCoS, UMR5259, 69621 Villeurbanne, France
[d] Department of Mechanical and Aerospace Engineering, Politecnico di Torino, Corso Duca degli Abruzzi 24, 10129 Torino, Italy
[e] Division LMSD Mecha(tro)nic System Dynamics, Department of Mechanical Engineering, KU Leuven, Celestijnenlaan 300, Box 2420, 3001 Leuven, Belgium
[f] Flanders Make@KU Leuven, Belgium
[g] Siemens Digital Industries Software NV, Interleuvenlaan 68, Leuven, Belgium
[h] Vrije Universiteit Brussel, Department of Mechanical Engineering, Pleinlaan 2, 1050, Brussels, Belgium
[i] University of Modena and Reggio Emilia, Via G. Amendola 2, 42122 Reggio Emilia, Italy
[j] PRISME - Eure-et-Loir Campus, 21 rue de Loigny-la-Bataille, 28000 Chartres, France
[k] UTC, Laboratoire Roberval, Compiègne, France
[l] Safran Aircraft Engines, France
[m] Safran Tech, Rue des Jeunes Bois, Châteaufort 78772 Magny–les–Hameaux, France
[n] Ecole Centrale de Lyon, LMFA, UMR5509, 69130, Ecully, France
[o] Laboratoire Quartz, ISAE-Supméca, 3 rue Fernand Hainaut 93400 Saint-Ouen, France
[p] Flanders Make@VUB, Belgium
[q] Safran Helicopter Engines, 64511 BORDES, France

ARTICLE INFO

Communicated by J. Slavič

Keywords:
High-speed video
Contest
Rolling element bearing

ABSTRACT

The aim of this paper is to provide a feedback on the signal processing contest organized at the Survishno/Resonance conference held in 2023 in Toulouse, France. The aim of the competition was to demonstrate the possibility of diagnosing a bearing operating at a variable rotation speed using high-speed video data only. To this end, a video of an operating faulty bearing was proposed to registered people a month before the event, with the task of extracting the instantaneous rotation speeds of the various rotating parts, and proposing a methodology for

* Corresponding author.
E-mail address: quentin.leclere@insa-lyon.fr (Q. Leclère).

https://doi.org/10.1016/j.ymssp.2025.112601
Received 3 October 2024; Received in revised form 12 March 2025; Accepted 15 March 2025
Available online 30 March 2025
0888-3270/© 2025 The Authors. Published by Elsevier Ltd. This is an open access article under the CC BY license (http://creativecommons.org/licenses/by/4.0/).

Fault diagnosis

identifying the type of fault (which was only known by the contest organizers). Ten teams of researchers from academia and industry were then formed, and proposed different approaches, the results of which were compared with reference data. The diagnostic task proved difficult, with none of the teams achieving the correct diagnosis of the fault. However, it is shown in this paper that by crossing the results of the different teams, it was possible to achieve the correct diagnosis. A tutorial is proposed at the end of the paper, presenting the application of a complete processing chain from video data to order envelope spectral analysis. Results illustrate the ability to recover bearing fault signatures, and also show the possibility to enhance the diagnosis by taking advantage of the fine tracking of the position of each part of the system offered by the video.

1. Introduction

The possibility of using video cameras in vibration analysis has become a popular topic during the last 15 years, due to the increase of storage capability, the development of video processing techniques related to computer vision and the decreasing costs of HS (high-speed) cameras. These approaches have already been investigated for modal analysis [1–4], operational vibration [5–11], or angular velocity measurements [12–19]. Few recent papers are dedicated to video-based rotating machinery fault diagnosis. Zhao et al. used motion magnification to detect vibrations induced by rotor unbalance or loosened anchor bolt on a rotating shaft [20]. Li et al. used a phase-based analysis of the optical flow to extract vibration signals from a faulty bearing operated at constant speed, managing to extract bearing fault features using envelope spectral analysis [21]. However, the possibility of extracting both vibration and rotation speed from a video in order to recover bearing fault features in varying speed conditions seems to remain unexplored. This last factual observation made this application a good candidate to be the topic of the contest organized at the Survishno 2023 conference (Resonance 2023, Toulouse). The contest took place in 2023 following the tradition of similar events organized previously by the community of rotating machines monitoring (CMMNO 2014, Surveillance 8 in 2015 and 9 in 2017, Survishno 2019). The contests are most of the time followed by a feedback paper summarizing the results and main findings [13,22,23]. These papers also generally came with a publication of the data, the object of the contest, for further use by the scientific community. It is interesting to note that these data sets are used quite intensively, as shown by the many publications that refer to them [24–38].

The present paper thus aims to report the Survishno 2023 contest, demonstrating the first implementation of video processing for REB (Rolling Element Bearing) diagnosis, and offering a support accompanying the contest data which are offered to the scientific community for further research. The object of the contest also relates to our limited knowledge of the erratic kinematic behavior of the bearing cage, which remains overlooked in mechanical models aimed at understanding bearing diagnostics (discussed for instance in a recent paper [24]). One objective of the contest consisted in addressing a major technical obstacle: How could a camera be used to observe, quantify, and potentially model the behavior of a bearing cage? Some observations and results are discussed throughout the paper to provide substantive answers to this question. The dataset of the contest is a HS video of a REB operating at varying speed, with an axial observation. The rotation of the different parts of the bearing (inner ring, outer ring, balls and cage) is clearly visible in the video. A fault was artificially introduced into the bearing for which determining the fault location was the main challenge of the competition. A total of ten teams from various countries, mainly academics but also a few industry professionals, submitted a contribution (see Table 1). Contributions of competing teams being the core of this paper, all active contributors are considered as co-authors.

Concerning the novelty of the work, the main targets are (1) to demonstrate that it is possible to access information on bearing faults from video analysis in nonstationary conditions, and (2) to show that bearing fault characteristics are improved by appropriate angular resampling that takes account of actual cage behavior, including slippage.

The paper is organized as follows. The experimental setup used for the video capture, as well as reference signals used to rank contestants' contributions, are described in the next Section 2. Contestant contributions are then investigated in Section 3, detailing the three speeds that had to be estimated (cage, shaft and outer ring). The possibility of identifying the fault signature from the contestant contributions is established in Section 4. Finally, a tutorial is proposed in a last Section 5, to illustrate a full processing chain from the video to the order envelope spectral analysis.

2. Studied system

2.1. Experimental setup

The studied bearing (SKF 6205 ETN9/C3) was mounted at one end of a shaft, driven at the other end by an electric motor through a flexible joint. The shaft was supported by two other lubricated bearings. The inner ring of the studied bearing had a tight fit on the shaft, while its outer ring was elastically attached to the frame through highly flexible springs (see Fig. 1). It should be noted that this quite unusual mounting was specifically chosen to allow quite large displacements, in order to ease the camera-based detection of fault-induced vibrations.

A HS camera (Phantom V710) was placed in front of the bearing, at about 1 m, and its optical axis was aligned with the shaft. The frame rate was set at 2 kHz, and each frame size was 800 × 800 pixels (see some frame samples in Fig. 2).

A camera output clock signal was recorded by an external data acquisition system, synchronized with sensors used to determine reference speed profiles (see Section 2.2), with a sampling frequency of 51200 Hz.

Table 1
List of competing teams.

Team name	Institution	Country
DIRG	Politecnico di Torino	Italy
SPHM	Safran tech/INSA Lyon/Univ. St Etienne	France
Le Tripot	Univ. of Modena/Univ. Orléans	Italy/France
Leuven A	KU Leuven/Flanders Make	Belgium
Leuven B	KU Leuven/Flanders Make/Siemens	Belgium
Meyo	Ecole Centrale Lyon	France
Poupon	Univ. de Tech. Compiègne	France
Shaft Watchmen	Safran Aicraft Engines	France
VAST-FM	ISAE-Supméca	France
VUB	Vrije Universiteit Brussel	Belgium

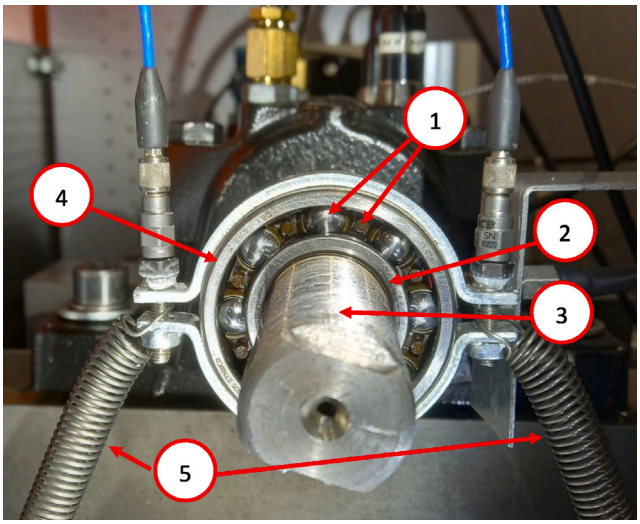


Fig. 1. Axial view of the studied bearing, with the 8 balls held in place by the cage (1). The inner ring (2) is mounted tightly on the shaft (3), the outer ring (4) attached to the frame through two springs (5).

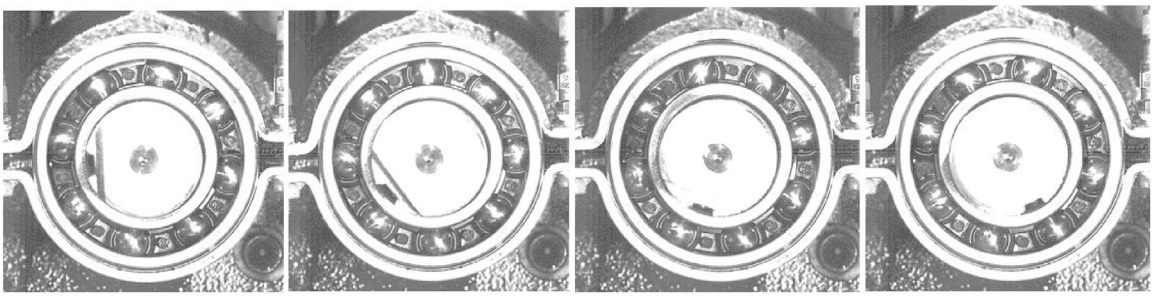


Fig. 2. Some consecutive frames captured by the HS camera.

2.2. Estimation of reference speed signals

The rotation speeds of the bearing's inner ring, outer ring and cage were estimated through dedicated sensors that serve as a ground truth for validating camera-based speed estimates. The different devices used to get reference signals are visible in Fig. 3. Signals were recorded with an 8 channels 24-bit OROS data acquisition system, at a sampling frequency of 51200 Hz, synchronously measured with the camera clock signal.

Zebra tapes with optical probes were used for the shaft and cage speed estimation, while an accelerometer was used for the outer ring. The latter was expected to oscillate around an equilibrium position with a small angular amplitude. Accelerometry was thus preferred to angular measurements. The accelerometer was fixed tangentially to the rotation degree of freedom, at a radius equal to 40 mm. Note that although two accelerometers are visible in the video and in Figs. 1 and 3, only one is used in the following. The acceleration signal was integrated to estimate the angular velocity of the outer ring. A high pass filter (f_c =3 Hz) was applied to

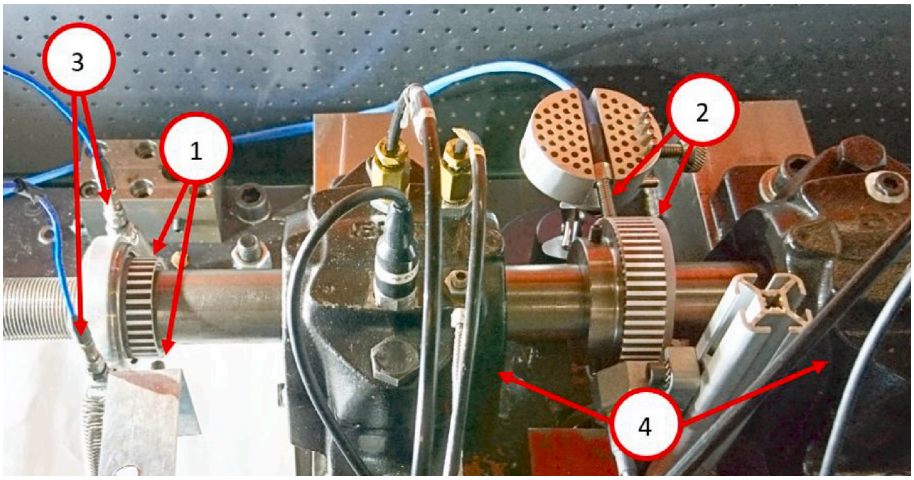


Fig. 3. Reference sensors on the bench: cage zebra tape with associated optical probe (1), shaft zebra tape with associated optical probe (2), accelerometers (3). The shaft is supported by the two main bearings (4).

the integrated signal, to prevent from amplification of low-frequency noise on acceleration data. The signal was then downsampled to the video frame rate (2 kHz).

A first zebra tape (adhesive tape with alternating white and black stripes) was classically pasted on an inertia wheel of the shaft, between the two main bearings, with a total number of 58 stripes. Mounting the second zebra tape on the cage was more challenging. A short piece of PVC tube with zebra tape (32 stripes) was directly glued on the cage, on the side offering a plane annular surface (see Fig. 3, left-hand side). The rotation speeds were kept relatively low to ensure negligible effects on the dynamic behavior of the bearing.

Zebra tape signals were processed with a dedicated algorithm taking into account the estimation of actual angular spacings between stripes [39]. A specific difficulty related to the use of zebra tapes is indeed the presence of an overlap zone between the two ends of the piece of tape, whose angle has to be estimated. This is done as follows: the rotation speed is first estimated using the entire revolution times for each stripe, whose passage over the optical sensor is determined by interpolating the upward zero-crossing of the signal. This revolution-averaged speed is then used to estimate the angles between each pair of stripes. Estimated angles are averaged over the entire non-stationary acquisition, and scaled to ensure that the total of angular spacings is strictly equal to 2π. A time-to-angle law $\theta(t)$ is finally established, for both cage and shaft.

The rotation speed of the shaft varies between 3 and 35 Hz, resulting in a time sampling rate of the rotation law between 175 and 2000 Hz. A similar analysis of the cage, that rotates at a frequency between 1 and 14 Hz, has a sampling rate between 32 and 450 Hz. Finally, these time-to-angle laws are interpolated using a regular time sampling defined by the clock signal of the video, to extract the angular position of the cage and shaft at each frame.

3. Analysis of contestant contributions

3.1. Contest rules and ranking indicators

The contest rules have been directly reproduced hereafter from the contest rule sheet that was initially published on the conference website:

> "The contestants shall estimate the instantaneous speeds of the shaft, the fundamental train (cage) and the outer ring. Additionally, the health condition of the bearing shall be diagnosed (...) The format of the contributions is a short presentation of 3 slides maximum for the speed estimation method, and 3 slides maximum for the bearing diagnosis. Additionally, the time history of the instantaneous angular speed for the shaft, fundamental train, and the outer ring (2000 samples by second in Hz) in a txt format should be provided".

These instantaneous speed files submitted by the competing teams have been used to rank the contributions by comparison with reference signals (of course not provided to contestants).

Contestants were thus asked to provide instantaneous speed signals with a time resolution identical to the video time resolution, i.e. a sampling frequency of 2 kHz. For the speed of the shaft and cage, the ground truth was based on the speed estimated from the zebra tapes, with their angular resolution defined by the respective number of stripes. The frequency bandwidth of the reference thus depends on the rotation speed (see previous section) and is always below 2 kHz. This means that the contestants' contributions cannot be analyzed beyond the resolution of the ground truth. In order to be as fair as possible, the following processing is applied to each contestants' contribution:

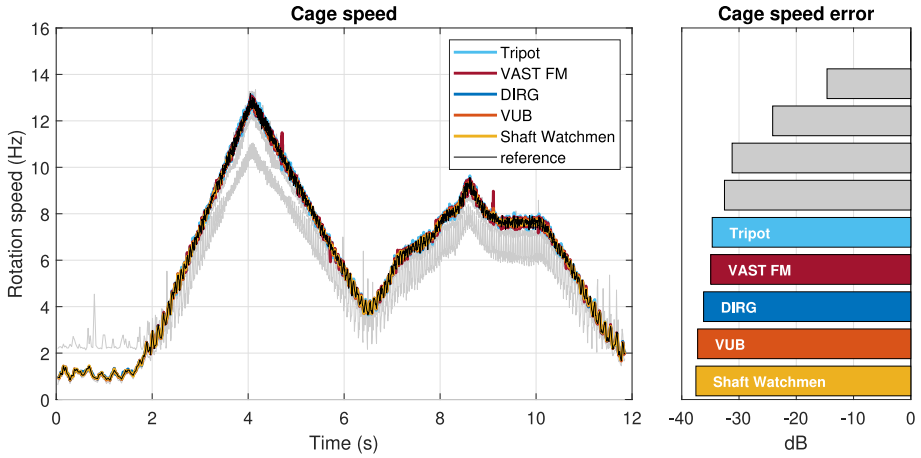


Fig. 4. Estimated cage speed signals compared to the reference (left). Corresponding error score (right). Colors correspond to the five contributions with the smallest errors, with the other teams in gray and the reference in black.

Table 2
Cage speed estimation: best scores and associated methods.

Rank	Team name	Error score (dB)	Method
1	*Shaft Watchmen*	−37.5	Reference frame detection
2	*VUB*	−37.2	Polar correlation
3	*DIRG*	−36.2	Pixel density distribution fitting

1. angular resampling using the reference time-to-angle law,
2. low pass filtering at $N/2$ epr (event per revolution), with N standing for the number of stripes,
3. downsampling at the angular resolution of the reference.

At the end, the score attributed to the contribution of contestant #i was based on the relative power of the speed error expressed as follows

$$\overline{e_i}^2 = \frac{\int_0^T \left(\dot{\theta}_i(t) - \dot{\theta}_{ref}(t)\right)^2 dt}{\int_0^T \left(\dot{\theta}_{ref}(t)\right)^2 dt} \approx \frac{\sum_n \left(\dot{\theta}_i[n] - \dot{\theta}_{ref}[n]\right)^2 / \dot{\theta}_{ref}[n]}{\sum_n \dot{\theta}_{ref}[n]}, \tag{1}$$

where T is the duration of the video, $\dot{\theta}_{ref/i}$ stands for the reference/contestant #i speed signal, t the time and n the sample index. The speed estimations of each of the bearing cage, shaft, and outer ring will be discussed in turn in the following sections.

3.2. Cage speed estimation

The contributions of competing teams concerning the estimation of the cage speed are compared to the reference in Fig. 4. The results are quite satisfactory considering that the seven best estimations obtain a score lower than −30 dB, the three best ones obtaining scores within a less than 2 dB margin. Interestingly, the approaches implemented by these three teams are radically different, as described hereafter.

The scores obtained by the three best contributions are gathered in Table 2, together with the methodology designation. The *Shaft Watchmen* team, obtaining the best score, used a two-steps method, based on a masked version of the video zeroed outside the zone of interest. The first step consists of estimating roughly the duration of 1/8 rotation by comparing each frame to the first one. Searching for local minima in a difference score gives frame indexes resembling to the first one (the cage is assumed to have an 8-order axial symmetry). The second step is based on the identification of a stabilized cycle (1/8 of rotation) at low speed, used to extract reference frames of the whole 1/8 of the cycle. Each frame of the video is finally compared to the reference frames in order to identify the corresponding position in the cycle. *Team VUB* first used a polar transformation of the video, in order to obtain a regular sampling in a (θ, r) grid. Then, an averaging is performed within the zone of interest (defined between two values of radius r), in order to get a signature of the cage as a function of θ, for each frame. A correlation is further estimated on the signatures of the different frames in order to estimate phase shifts in θ. *Team DIRG* implemented a radically different approach, based on a pixel density fitting method. Once a region of the frame is selected, a pixel density distribution is extracted onto which a proper reference distribution is fitted to extract the angular position information that optimizes the fitting.

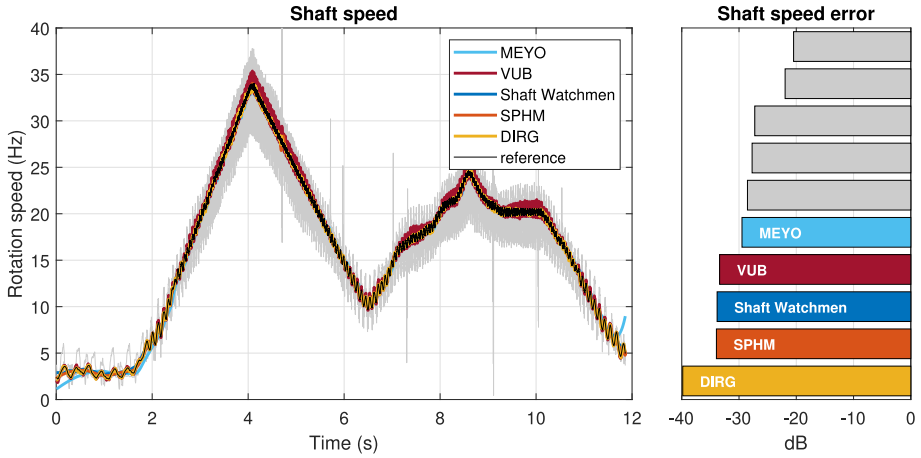


Fig. 5. Estimated shaft speed signals compared to the reference (left). Corresponding error score (right). Colors correspond to the five contributions with the smallest errors, with the other teams in gray and the reference in black.

Table 3
Shaft speed estimation: best scores and associated methods.

Rank	Team name	Error score (dB)	Method
1	*DIRG*	−39.8	Template-Matching
2	*SPHM*	−33.9	Virtual speed sensors
3	*Shaft Watchmen*	−33.8	Reference frame detection

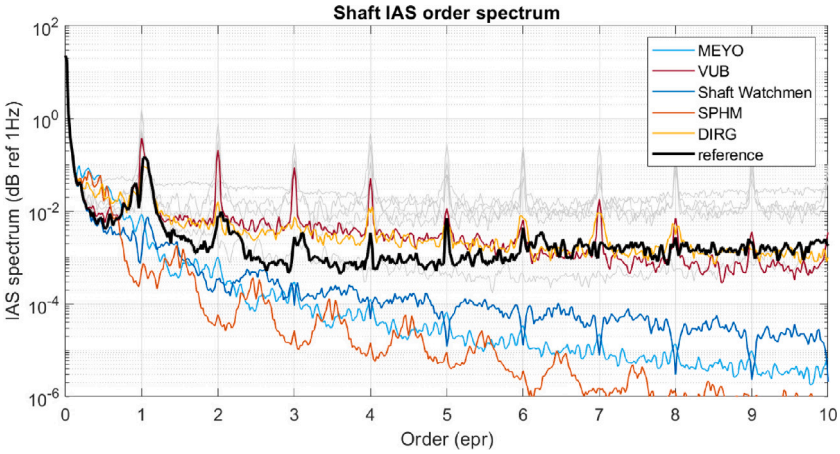


Fig. 6. Shaft order spectrum for reference (black) and recovered from the video (five best estimations in colors, other teams in gray and the reference in black).

3.3. Shaft speed estimation

The contributions of competing teams concerning the estimation of the shaft speed are compared to the reference in Fig. 5.

It is worth noting that similar methodologies have been implemented by most of the teams for identifying the shaft or cage speeds. It is thus not surprising to find the teams on the podium of the cage at the first places also for the shaft, yet with a different ordering (see Table 3). Team *SPHM* also provided a good contribution, obtaining the second lowest error score for the shaft. *team DIRG* used a specific template-matching method for the shaft case, based on their previous work [40]. The idea is to set-up a reference shape (binary, i.e. black and white), called template, whose parameters (position, thickness, rotation) are optimized for each frame (also binarized). Interestingly, this template matching method significantly outperforms other ones by at least 6 dB. This might be related to the effect of the lighting. It is indeed visible, when watching the video, that the details, and especially the details of the shaft's end, are modulated by the lighting of the scene, at an order equal to the rotation speed of the shaft. The order amplitude spectra of the identified and reference shaft speed are drawn in Fig. 6.

Most of the estimated shaft speeds exhibit strong harmonics at integer orders, that are not present in the spectrum of the reference. This confirms the significant contribution of lighting artifacts, to which a majority of approaches are highly sensitive. Four among the

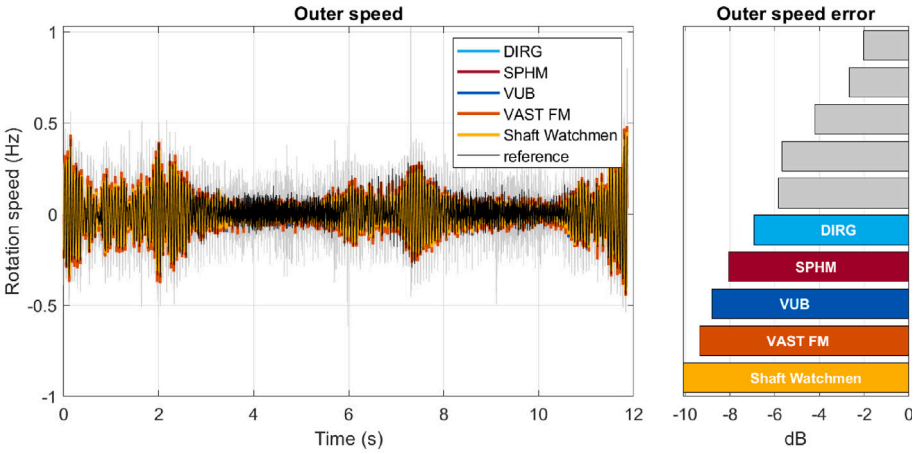


Fig. 7. Estimated outer ring speed signals compared to the reference (left). Corresponding error score (right). Colors correspond to the five contributions with the smallest errors, with the other teams in gray and the reference in black.

Table 4
Outer ring speed estimation: best scores and associated methods.

Rank	Team name	Error score (dB)	Method
1	*Shaft Watchmen*	−10.1	Color threshold crossing
2	*VAST-FM*	−9.4	Lucas kanade optical flow
3	*VUB*	−8.8	Polar correlation

five best estimations are much less affected by those harmonics. The estimation of the *Shaft Watchmen* team clearly exhibits symptoms of a CS1-removal filter (subtraction of the synchronous average of one shaft revolution) : this part of the signal was indeed identified by this team as a potential source of error. Contributions of *SPHM* is quite good at low order, but strongly underestimated above order 1. *SPHM* used some pixels as *virtual speed sensors*, to detect the passage of specific object. *MEYO* used a well known computer vision object tracking algorithm (YOLOv5 [41]). These approaches are not sensitive to lighting effects, contrary to correlation based methods. This is confirmed by the outperforming *DIRG* result. The spectrum of the shaft speed obtained by this team is indeed very close to the reference one up to order 10, without being strongly disturbed by integer orders. This good result may also be explained by the "tracking" nature of the template-fitting procedure, based on binarized images, that finally revealed to be more robust to lighting effects than the other methods.

3.4. Outer ring speed estimation

Contestants' contributions concerning the estimation of the outer ring speed are given in Fig. 7, together with the reference estimated using an accelerometer. The outer ring was not rigidly clamped to the frame, but attached to it through low stiffness springs, allowing a significant motion in rotation around the shaft axis. The speed reaches almost a 0.5 Hz amplitude, with a strong component at 16.5 Hz due to the resonance of the inertia-spring mode (well observed on Fig. 9). This resonance is mainly excited by integer orders of the shaft rotation speed. This is particularly clear around time stamps 6 and 7 s, when the shaft speed (order 1) crosses the resonance frequency successively downward and upward (see Fig. 5). At the beginning and end of the record, the resonance is excited by higher integer orders.

The scores and methods of the three best contributions are given in Table 4. Once again, the best score is obtained by the *Shaft Watchmen*, with an error of −10 dB. The approach implemented by this team is quite simple, based on the analysis of a small subpart of the video, smartly interpreted by averaging the image over one dimension before applying a threshold detection. The procedure is illustrated in Fig. 8. *Team VAST FM* also reached a good error score, using a completely different method based on the Lucas Kanade Optical Flow [42]. Twenty points are 'followed' in the region of the picture associated to the outer ring, and the rotation is assessed using a least mean squares estimate. The third best score is obtained by *team VUB*, using a cross-correlation approach based on a polar transformation of images. It is noteworthy that teams *VUB* and *DIRG* implemented the same methods (template-fitting for *DIRG*, polar correlation for *VUB*) to estimate either the shaft or outer ring rotation speeds, albeit with different levels of estimation accuracy. The correlation approach seems to be more efficient to track targets oscillating around a fixed position (which is the case of the outer ring), while template-fitting would be more robust to lighting modulation caused by large target displacements.

The fact that the outer ring rotation is of zero mean makes it a good candidate for further analysis of its frequency content, especially for diagnosis purpose as conducted in the following section. It is thus interesting to look at the contestants' contributions in the frequency domain and to compare them with the reference (estimated with the accelerometer), as shown in Fig. 9. The figure is displayed in logarithmic scale, in order to highlight the very good agreement obtained in the low-frequency range (up to 20

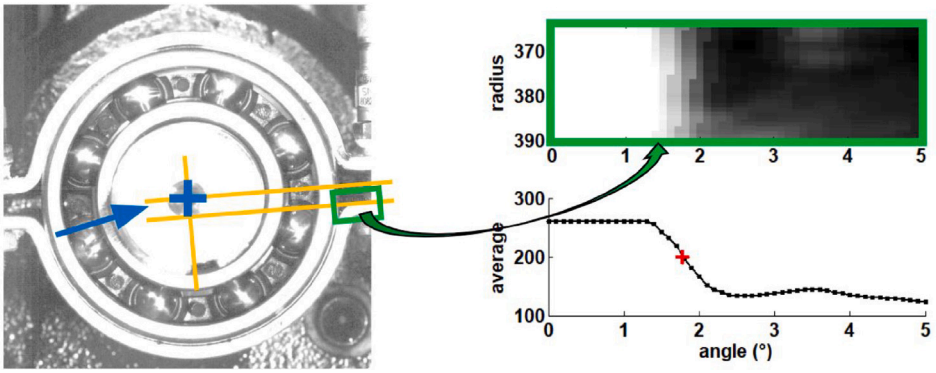


Fig. 8. Estimation of the outer ring vibration (*Shaft Watchmen team*) : location of the rotation axis (left), analysis of a sub-image by radial averaging and thresholding (right).

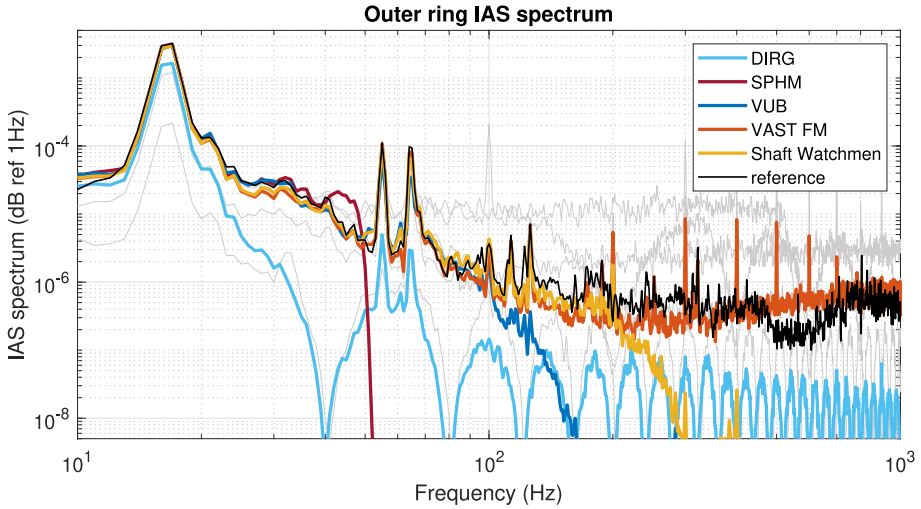


Fig. 9. Power spectrum of the outer ring speed signal. Contestants' contributions estimated from the video (five best in colors, other ones in gray), against the reference estimated from the accelerometer (black).

to 200 Hz depending on the team). However, the deviation from the reference becomes quite huge in the high-frequency range, either because of a strong low-pass filtering (teams *SPHM*, *VUB* or *Shaft Watchmen*) or a strong harmonic noise related to 100 Hz and harmonics (*VAST FM* and others in gray). The latter is probably related to a lighting modulation caused by the lighting power supply.

4. Bearing fault analysis

A severe localized fault was artificially introduced on the inner ring of the bearing. This fault generates a train of pulses corresponding to the ball pass frequency, defined in angle as one eighth of the relative rotation of the shaft with respect to the cage. The rotation speed of the cage is known from the kinematic analysis of the bearing with perfect rolling conditions, allowing the determination of so-called bearing frequencies. The frequencies of the studied bearing (SKF 6205ETN9), as given by the manufacturer, are given in Table 5. The frequencies are expressed in epr of the relative rotation of the inner ring to the outer ring.

4.1. Bearing diagnostics based on reference signals

Reference signals are used at first to show the signature of the fault, that is strongly contributing to the accelerometer signal. In the present case, the outer ring average rotation speed is zero. The angular acceleration of the outer cage, directly estimated through the accelerometer (still band-pass filtered between 3 and 1000 Hz) is first resampled in angle using the reference speed of the shaft. The envelope order spectrum is drawn in Fig. 10 (blue). The family of harmonics at integer multiples of the BPFI ($k\times4.982$) significantly emerges from the integer harmonic comb. The phenomenon is even better caught when resampling the vibration with

Table 5
Characteristic frequencies of the studied bearing, in event per revolution of the relative inner ring to outer ring rotation speed.

Bearing events	Epr
Ball pass frequency on the inner ring	4.982
Ball pass frequency on the outer ring	3.018
Ball spin frequency	1.914
Cage rotation speed wrt outer ring	0.377

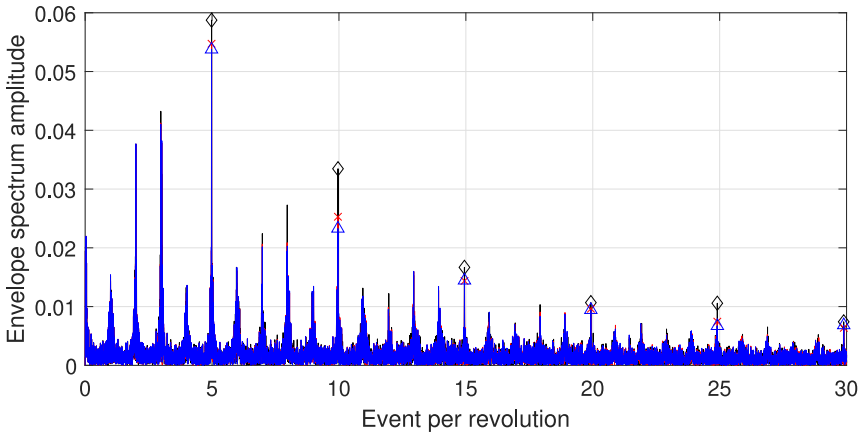


Fig. 10. Order envelope spectrum of the outer ring acceleration (reference) with respect to the shaft's rotation. Vibration signal resampled in angle of the shaft (blue and triangles), resampled in angle of the shaft relatively to the outer ring's angle (red and x), and resample in angle of the cage relatively to the outer ring's angle (black and diamonds). Markers show the maximum reached at the fault frequencies.

respect to the relative rotation of the shaft with respect to the outer ring (that oscillates because of its flexible connection to the frame). The resulting envelope spectrum is drawn in Fig. 10 (red). Ultimately, one can take advantage of the knowledge of the measured rotation of the cage. The BPFI value is indeed physically related to the rotation of the shaft with respect to the cage, with a number of pass over the defect for each relative revolution equal to the number of rolling elements. The vibration signal is finally resampled using the rotation of the shaft speed with respect to the cage. The resulting order spectrum is drawn in Fig. 10 (black), still as a function of the orders of the shaft rotation (shaft to cage orders are converted to shaft orders by a multiplication by the ratio of average speeds). The harmonicity of BPFI-related events is once again clearly improved, a symptom of imperfect rolling related to the "cage slippage" phenomenon, justifying a diagnostic of the REB accounting for the real fundamental train speed (see [24] for a detailed overview).

4.2. Bearing diagnostics from contestant contributions

The task of identifying the fault from the video data only turned out to be quite a difficult one, with none of the contestants able to definitively detect the fault. Based on contestants' contributions, there was yet a possibility to implement a similar analysis as the one proposed in Section 4.1 (based on reference signals). To do so, it was first necessary to differentiate the estimated outer ring speeds to obtain the outer ring accelerations. Then, it was possible to resample this vibration signal with respect to the estimated shaft-cage relative rotation.

In order to understand the main issues of this processing, it is decided to first analyze the reference vibration signal resampled with respect to the best contestant estimation of the shaft speed (contribution of *team DIRG*), and then to analyze the best estimation of the outer ring speed (contribution of *team Shaft Watchmen*) with the reference speed. The results are shown in Fig. 11. The reference acceleration resampled with video-estimated speeds (left) clearly exhibits similar features as the one resampled with the reference signals (Fig. 10). On the other hand, the resampling of the best video-estimated acceleration with reference speed profiles leads to a very noisy envelope spectrum. The first harmonic of the fault frequency comb still emerges significantly, but its amplitude, as well as the overall amplitude of the spectrum, is strongly attenuated. This is easily explained by looking at the frequency content of the video-based signals (see Fig. 9): the high-frequency part is not well estimated. This part of the spectrum being likely to carry the main features of the fault signature (cf. [43]), the degraded estimation of the signal from video data makes diagnosis difficult.

Ultimately, it was an objective of the contest to demonstrate the possibility to perform a successful bearing diagnosis solely from the video data. While none of the teams have reached this objective individually, it was possible to merge the best outer race, shaft and cage estimates to achieve a collegial result.

The outer ring acceleration has to be resampled with respect to the relative shaft/cage position. The best outer ring vibration is obtained by team *Shaft Watchmen*. Concerning the identification of cage and shaft positions, it appears that the most reliable

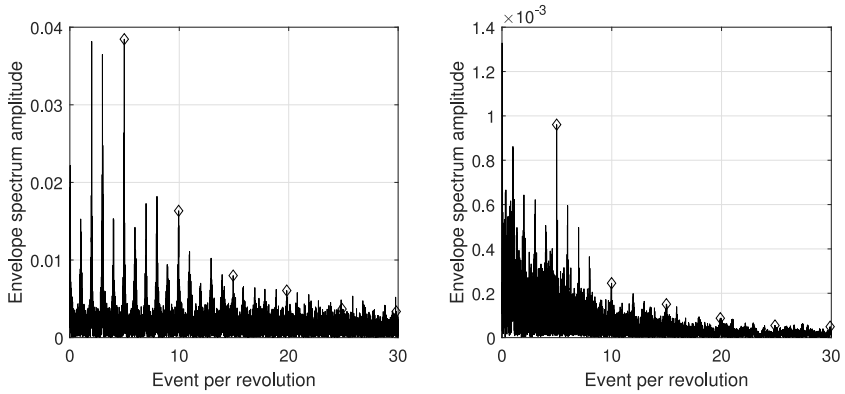


Fig. 11. Order envelope spectrum of the outer ring acceleration with respect to the shaft orders. Reference outer ring acceleration resampled with respect to the best shaft speed signal (left), and best outer ring signal resampled with reference shaft speed (right). Markers show the maximum reached at the fault frequencies.

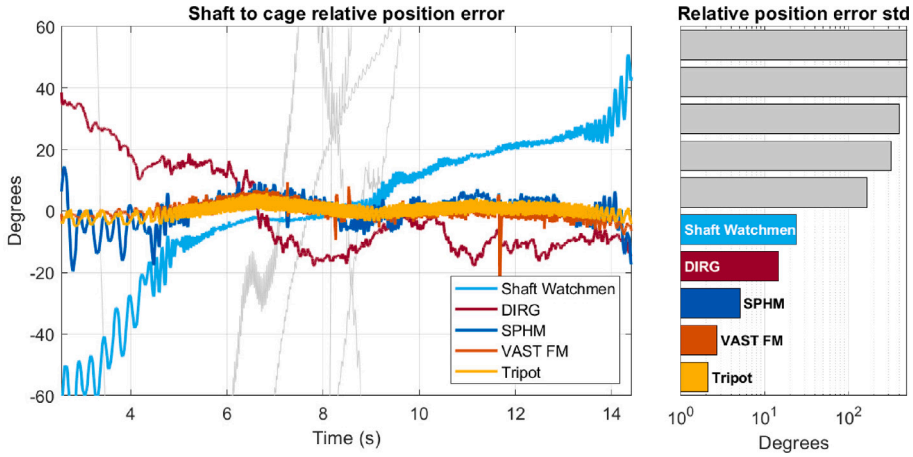


Fig. 12. Shaft to cage relative position error in degrees (centered). Corresponding standard deviation (right). Colors correspond to the five contributions with the smallest standard deviations, other ones in gray.

contributions are not the ones that reached the most reliable speeds. Contestant were asked to provide instantaneous speeds signals, and were evaluated on it. However, when integrating these speeds to get the angular positions, some large deviations are observed on several contributions as compared to the reference. These observations are illustrated in Fig. 12, in which the difference between the reference shaft-to-cage position and the contributions of contestants are drawn in degrees (left), together with the corresponding standard deviations (right). Clearly, some of the contributions are strongly deviating, with a cumulative error of several shaft to cage revolutions between the beginning and the end of the video recording. It is worth noting that such large deviations will inevitably lead to break the periodicity of resampled signals. Three contributions show a quite good position estimation all along the record, with a standard deviation lower than 3 degrees. These good estimation of the position is due to the fact that these teams actually deduced the speed of the shaft from the estimation of its position, while other teams directly estimated the speed without verifying that its integration was consistent with the position.

The contribution of the *Tripot team* is finally used to obtain the shaft and cage angular position information to resample the outer ring acceleration from team *Shaft Watchmen*, which was previously high-pass filtered at 20 Hz. The envelope spectrum of the result is drawn in Fig. 13. The fault signature clearly shows up in this spectrum, demonstrating the possibility of identifying it directly from video processing.

5. Tutorial: processing the contest video to extract bearing fault features

In this section, the description of a full processing implementation is proposed, from the raw video data to envelope order spectrum analysis. It should be noted that this description is deliberately written simple and wordy, with no equations or algorithms. For the reader who wishes to go into more technical detail, this section is accompanied by a functional ready-to-use Jupyter notebook, attached as supplementary material, that is readily applicable to the video file (that is published in a dedicated repository [44]). This notebook is structured in 6 steps constituting cells of code. The role of each step is described hereafter.

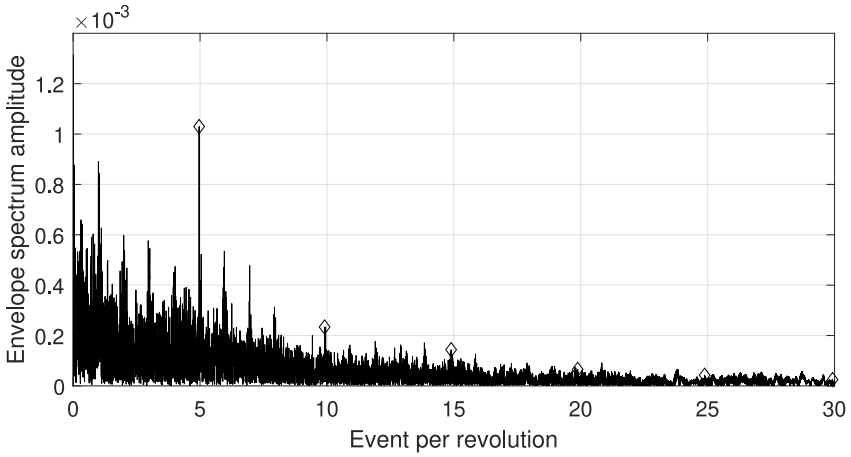


Fig. 13. Order envelope spectrum of the outer ring acceleration with respect to the shaft's rotation, estimated from the video data only. Vibration signal from team *Shaft Watchmen* resampled in angle of the cage relatively to the outer ring from *Tripot team*. Markers show the maximum reached at the fault frequencies.

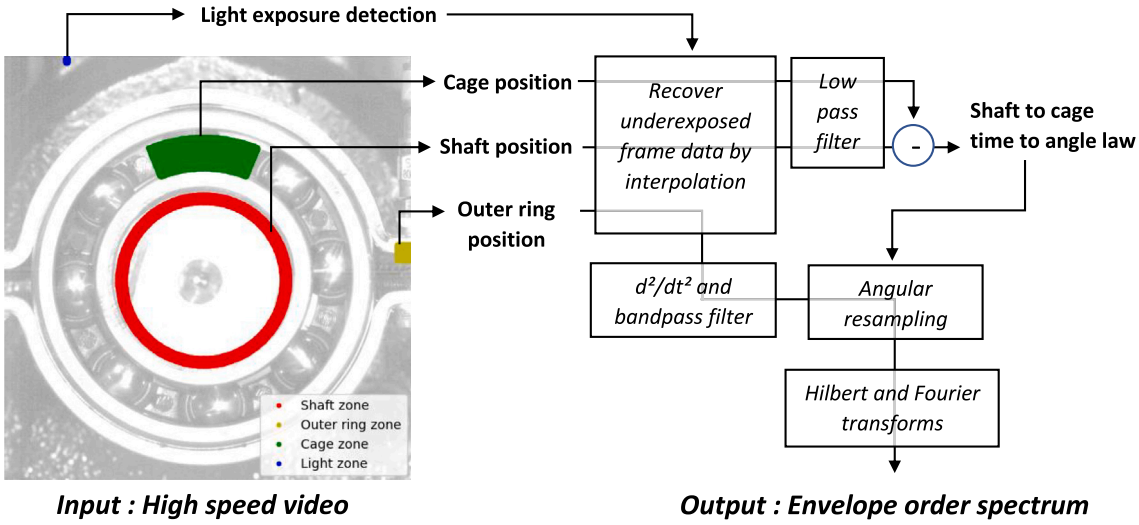


Fig. 14. Complete processing chain proposed in this tutorial, from the specific zones of interest on the video, used as virtual sensors, to the envelope order spectrum used for the diagnosis.

The first step consists in extracting different zones from the video, used in the following as virtual sensors to estimate the different quantity of interest. These zones are represented in Fig. 14:

- A first small zone on the upper left side of the image focuses on a detail of the background strongly varying with the lighting modulation: this will allow to identify and reject frames with a strong lighting bias.
- The second zone on the right side focuses on a detail of the outer ring with a sharp black to white transition from the background to the tracked object. This will be used to extract the angular vibration of the outer ring.
- The third zone consists of a ring of the shaft section containing the notch, that will be tracked to estimate the shaft position.
- The fourth zone is a sector of 1/8 of the cage chosen to track the cage position. The cage having a periodic pattern of 1/8 rotation, the position of the pattern is tracked over this angular range only.

Note that the two latter zones are interpolated on polar grids, using a nearest-like interpolation. Another indicator is also picked up for each frame: the number of pixels with a zero value. This will allow later to easily identify frames with an acquisition problem.

The second step is to identify frames subject to a lack of lighting or to an acquisition issue. Under-exposed frames are identified by thresholding the average gray level on the first zone of interest. This leads to a rejection of 2886 frames (about 12% of the total number of frames). Frames with an acquisition problem are identified by an abnormally high number of black pixels. 134 frames with a number of black pixel greater than 30 are considered as defective. Finally, only 20836 frames are considered in the following for the processing.

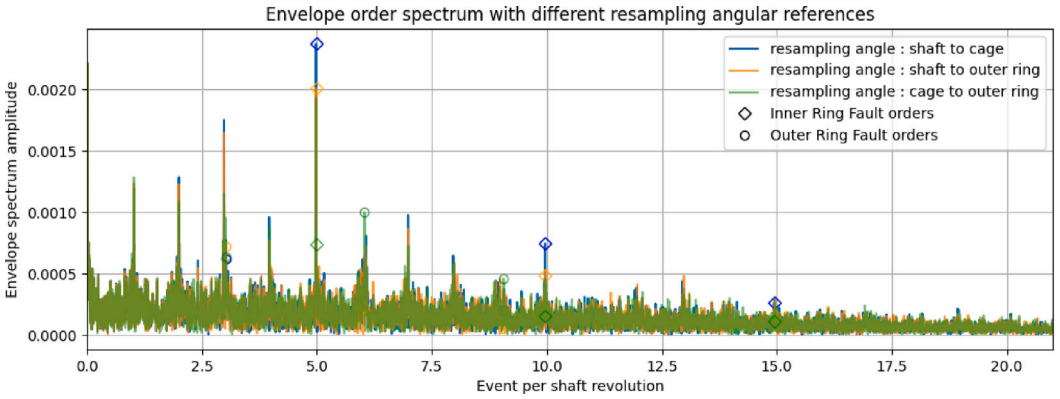


Fig. 15. Envelope order spectrum of the outer ring acceleration with respect to the shaft's rotation (output of the tutorial).

The third step is to process the zone used to extract the outer ring vibration. The angular displacement of the outer ring is quite small, the targeted detail of the scene is thus not that much affected by the anisotropy of the lighting. Each column of the zone of interest consists of a number of bright pixels (the target) followed by dark pixels (the background). The transition from bright to dark is set to a given threshold (the value of 180 is used in the following) whose vertical position is determined by linear interpolation. These positions are then averaged over all the columns of the zone. The average position (in pixels) is converted in angle by dividing it by the average radius of the zone (average distance to the shaft axis).

The fourth step deals with the estimation of the shaft angular position for each frame. This task is a bit more complicated, as the tracked detail aspect (the notch on the shaft ending) is severely affected by the light orientation. A specific pattern representing the notch is artificially generated, and then searched by scanning the whole angular range from 0 to 2π and maximizing the correlation with the image. The angle of the shaft during the whole video is then obtained by unwrapping the angular position.

In a fifth step, a similar process is implemented for the cage, except that the pattern is obtained by thresholding a specific frame of the video, and that it is correlated with all other frames over a scanning angle of one eight of revolution only, considering the circular symmetry of order 8 of the cage. The angle of the cage is then obtained by unwrapping the angular position - with a specific unwrapping period of $2\pi/8$.

Finally, the last step is dedicated to angular resampling and Fourier analysis. Different angular references can be chosen, the shaft-to-cage, the shaft-to-outer ring, or the cage-to-outer ring angles. Considering a possible sliding between the different elements of the bearing, these references could lead to different results. The shaft-to-cage (resp. cage-to-outer ring) angle is to be preferred for inner ring (resp. outer ring) faults, while the shaft-to-outer ring is the classical resampling reference (based on a no-sliding hypothesis). The three aforementioned cases are considered here. The outer ring angular position is derived 2 times to get an angular acceleration, and then band-pass filtered between 20 and 500 Hz. It is then resampled in angle with respect to the chosen reference, and then processed classically by successively applying Hilbert and Fourier transforms to get the envelope spectrum. The result obtained considering the three possible angular references are drawn in Fig. 15. Note that the envelope spectra are all scaled in order of the shaft revolution to ease their comparison, by multiplying the order of the chosen reference with the average speed ratio to the shaft.

The analysis of these envelope spectra confirms at least two facts. Firstly, the inner ring fault order is clearly and strongly emerging, confirming the presence of an IR fault. Secondly, the choice of the angular reference has a significant effect on the fault signature, which is clearly maximized in this case with respect to the shaft-to-cage angular relative displacement, confirming results obtained with reference signals (see Section 4.1). This means that the hypothesis of non-sliding between bearing parts is not respected here. This can be illustrated by the sliding angle of the cage, defined here as the time evolution of the angle difference between the theoretical position of the cage (estimated from the shaft position and a no-sliding hypothesis), and the actual position. This sliding angle is drawn in Fig. 16 together with the shaft rotation speed. It can be seen that the sliding amplitude is not that important (variation amplitude of about 15 degrees), but this is enough to degrade the fault features when using the classical no-sliding hypothesis. Also, it is interesting to correlate at least qualitatively the sliding with the acceleration of the shaft. Clearly, the two main run-up and coast-down are inducing a negative and positive sliding, which could be consistent with sliding induced by inertial effects. A deeper analysis of this phenomenon is left for future work.

6. Conclusion

The aim of this section is to provide some concluding remarks on the results presented in this paper, and more generally on the competition that gave rise to this work. The initial aim of the competition was to evaluate the possibility of diagnosing bearing defects using HS video. The competition format enabled different approaches to be compared objectively and new ideas to be generated from a wide range of researchers, all in a stimulating and fun spirit of competition. The task required of the participants

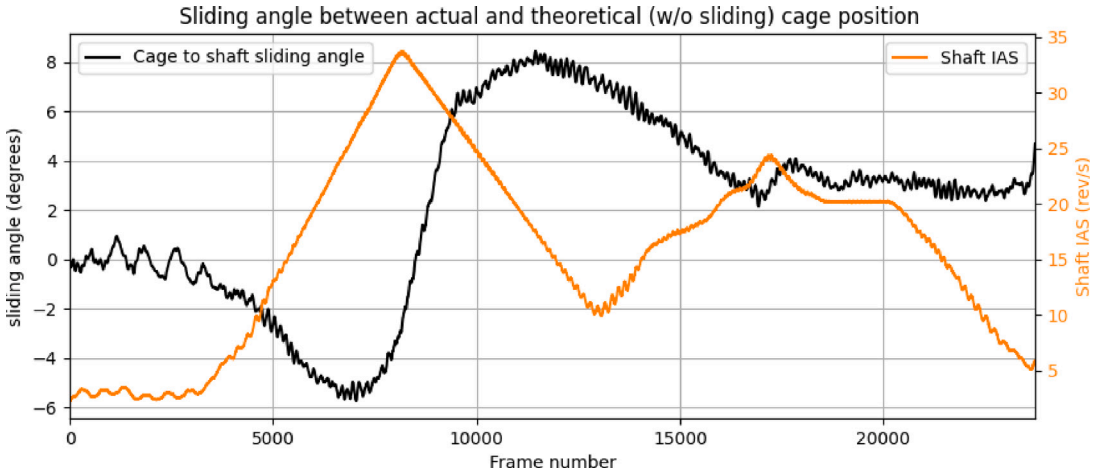


Fig. 16. Time evolution of the cage to shaft sliding angle (black) together with Shaft Instantaneous angular speed (orange).

was twofold: to extract from the video the instantaneous rotational speeds of the various moving parts, and to carry out the correct diagnosis of the faulty bearing under investigation.

The competitors' contributions to the first task highlighted the advantages and disadvantages of the proposed solutions. We can draw two main conclusions:

- methods based on image correlation have proved to be particularly efficient in terms of spatial resolution, but also highly sensitive to the problems of lighting fluctuations (fluctuations in intensity linked to the power supply, but also and above all spatial inhomogeneity of lighting generating periodic fluctuations in the image of a rotating object),
- methods based on source recognition and tracking algorithms have proved to be more robust in the face of the lighting problems mentioned above, albeit with less accurate results.

As for the diagnostic task, it proved more difficult considering the participants' inability to correctly identify the fault. However, this paper shows that it was still possible to diagnose the fault using only high-speed video, and only using contestant contributions, by cross-analyzing the speeds provided by different teams. A complete processing chain, strongly inspired by the methods implemented by the contestants, has been described in this work.

Main findings are listed hereafter:

- one major advantage of video diagnostics lies in the ability to capture the actual position of the cage relatively to the rings,
- the main difficulty with video-based bearing diagnostics lies in its limited access to the high frequency range.

The first point opens the door to angular resampling with respect to the true cage to ring angles, thus getting rid of the cage-slipping blurring effect observed in classical approaches. The second point is related to the limited time resolution of HS cameras as compared to standard sampling rates used in vibration analysis, but also to the fact that the video sensor is actually a displacement/position sensor, making it much more difficult to access the high frequency content of the vibration spectrum as compared to accelerometry — this high frequency range is known to carry information about bearing faults. The fact that bearing fault signatures are generally detected at high frequencies, for example by analyzing an accelerometer envelope spectrum. The video camera is in fact a displacement sensor, necessarily more limited in sampling frequency than a conventional acquisition system. Access to high-frequency information is therefore much more difficult as compared to classical approaches based on accelerometer measurements. As a perspective, it could be interesting to mix accelerometry and HS camera acquisition in order to take advantage of both approaches.

Finally, it can be concluded that the main targets of the work have been reached. First, the possibility to establish a diagnosis of a bearing operating in nonstationary conditions from video data only has been clearly demonstrated. Second, it is shown that the possibility to track the position of each element of the bearing offered by the video capture constitutes a significant added value as compared to classical approaches. In the particular case studied in this work, the angular resampling with respect to the shaft-to-cage angle has clearly enhanced the signature of the fault as compare to classical resampling with respect to the shaft only.

CRediT authorship contribution statement

Quentin Leclère: Writing – original draft, Supervision, Project administration, Investigation, Data curation. **Hugo André:** Writing – review & editing, Supervision. **Jérôme Antoni:** Supervision. **Arthur Burel:** Writing – review & editing, Investigation, Data curation. **Cécile Capdessus:** Writing – review & editing, Investigation. **Marco Cocconcelli:** Writing – review & editing, Investigation.

Gianluca D'Elia: Writing – review & editing, Investigation. **Alessandro Paolo Daga:** Writing – review & editing, Investigation. **Jean-Luc Dion:** Writing – review & editing, Investigation. **Mohammed El Badaoui:** Writing – review & editing, Investigation. **Abdallah El Hidali:** Writing – review & editing, Investigation. **Luigi Garibaldi:** Writing – review & editing, Investigation. **Julien Griffaton:** Writing – review & editing, Investigation. **Konstantinos Gryllias:** Writing – review & editing, Investigation. **Yunhyeok Han:** Writing – review & editing, Investigation. **Jan Helsen:** Writing – review & editing, Investigation. **Fadi Karkafi:** Writing – review & editing, Investigation. **Kayacan Kestel:** Writing – review & editing, Investigation. **Layla Kordylas:** Writing – review & editing, Investigation. **Deepti Kunte:** Writing – review & editing, Investigation. **Stefania Lo Feudo:** Writing – review & editing, Investigation. **Adrien Marsick:** Writing – review & editing, Validation, Methodology, Investigation, Data curation, Conceptualization. **Douw Marx:** Writing – review & editing, Investigation. **Alex Ricardo Mauricio:** Writing – review & editing, Investigation. **Johann Miranda-Fuentes:** Writing – review & editing, Investigation. **Cédric Peeters:** Writing – review & editing, Investigation. **Thomas Poupon:** Writing – review & editing, Investigation. **Didier Rémond:** Supervision. **Franck Renaud:** Writing – review & editing, Investigation. **Julien Roussel:** Writing – review & editing, Investigation. **Jimmy Touzet:** Writing – review & editing, Investigation, Data curation. **Toby Verwimp:** Writing – review & editing, Investigation. **Luca Viale:** Writing – review & editing, Investigation. **Mahsa Yazdanianasr:** Writing – review & editing, Investigation. **Rui Zhu:** Writing – review & editing, Investigation.

Declaration of competing interest

The authors declare that they have no known competing financial interests or personal relationships that could have appeared to influence the work reported in this paper.

Acknowledgments

This work was performed within the framework of the Labex CeLyA of Université de Lyon, operated by the French National Research Agency (ANR-10-LABX-0060/ ANR-11-IDEX-0007). Fadi Karkafi, Deepti Kunte and Douw Marx gratefully acknowledge the European Commission for its support of the Marie Skłodowska Curie program through the ETN MOIRA project (GA 955681). Toby Verwimp would like to acknowledge the support of the Fonds Wetenschappelijk Onderzoek Vlaanderen (FWO) under the FWO strategic basic research grant no. 1SE0123N. Rui Zhu and Konstantinos Gryllias would like to acknowledge Flanders Make, the strategic research center for the manufacturing industry, and VLAIO in the context of the FM SBO QED project. Alex Ricardo Mauricio, Mahsa Yazdanianasr, Konstantinos Gryllias, Kayacan Kestel, Cédric peeters, and Jan Helsen would like to acknowledge the support of the Fonds Wetenschappelijk Onderzoek Vlaanderen (FWO) under the FWO Strategic Based Research project no. S006119N Robustify. Jan Helsen and Cédric Peeters would like to thank AI Flanders for the support. VUB would like to thank the Blue Cluster in Belgium for supporting their researchers through the Supersized 5.0 project.

Appendix A. Supplementary material

The datasets used in this work are shared publicly on a zenodo repository [44]. It consists of the video of the contest itself, accompanied by the time data of the reference signals. Please cite this paper and the reference to the dataset for any subsequent publication exploiting it. https://zenodo.org/records/13707571.

A Jupyter notebook with python code is also appended to this paper as supplementary material. This notebook is a ready-to-use processing code that can be directly applied to the shared video to get the results discussed in the last section.

Appendix B. Supplementary data

Supplementary material related to this article can be found online at https://doi.org/10.1016/j.ymssp.2025.112601.

Data availability

The data is already shared on a public repository.

References

[1] Y. Wang, F.S. Egner, T. Willems, M. Kirchner, W. Desmet, Camera-based experimental modal analysis with impact excitation: Reaching high frequencies thanks to one accelerometer and random sampling in time, Mech. Syst. Signal Process. 170 (2022) 108879, http://dx.doi.org/10.1016/j.ymssp.2022.108879, URL https://www.sciencedirect.com/science/article/pii/S0888327022000723.

[2] J. Javh, J. Slavič, M. Boltežar, High frequency modal identification on noisy high-speed camera data, Mech. Syst. Signal Process. 98 (2018) 344–351, http://dx.doi.org/10.1016/j.ymssp.2017.05.008, URL https://www.sciencedirect.com/science/article/pii/S0888327017302637.

[3] F. Renaud, S. Lo Feudo, J.-L. Dion, A. Goeller, 3D vibrations reconstruction with only one camera, Mech. Syst. Signal Process. 162 (2022) 108032, http://dx.doi.org/10.1016/j.ymssp.2021.108032, URL https://www.sciencedirect.com/science/article/pii/S0888327021004258.

[4] J.G. Chen, N. Wadhwa, Y.-J. Cha, F. Durand, W.T. Freeman, O. Buyukozturk, Structural modal identification through high speed camera video: Motion magnification, in: J. De Clerck (Ed.), Topics in Modal Analysis I, vol. 7, Springer International Publishing, Cham, 2014, pp. 191–197.

[5] J.G. Chen, N. Wadhwa, Y.-J. Cha, F. Durand, W.T. Freeman, O. Buyukozturk, Modal identification of simple structures with high-speed video using motion magnification, J. Sound Vib. 345 (2015) 58–71, http://dx.doi.org/10.1016/j.jsv.2015.01.024, URL https://www.sciencedirect.com/science/article/pii/S0022460X1500070X.

[6] Y. Yang, C. Dorn, T. Mancini, Z. Talken, G. Kenyon, C. Farrar, D. Mascareñas, Blind identification of full-field vibration modes from video measurements with phase-based video motion magnification, Mech. Syst. Signal Process. 85 (2017) 567–590, http://dx.doi.org/10.1016/j.ymssp.2016.08.041, URL https://www.sciencedirect.com/science/article/pii/S0888327016303272.

[7] H. Jasim, J. Alsalaet, Detecting vibration problems in machines and structures using motion capturing by camera, Basrah J. Eng. Sci. 21 (2021) 38–49, http://dx.doi.org/10.33971/bjes.21.1.6.

[8] S. Cao, H. Nian, J. Yan, Z. Lu, C. Xu, Modal analysis and damage localization in plate-type structures via tdd and pe methods based on the data of an integrated highspeed camera system, Mech. Syst. Signal Process. 178 (2022) 109309, http://dx.doi.org/10.1016/j.ymssp.2022.109309, URL https://www.sciencedirect.com/science/article/pii/S0888327022004472.

[9] G. Paunescu, P. Lutzmann, D. Wegner, B. Göhler, Detecting vibration features from remote objects based on high-speed imagery, Opt. Eng., Bellingham 60 (2021) 013102, http://dx.doi.org/10.1117/1.OE.60.1.013102.

[10] L. Breńkacz, P. Bagiński, G. Zywica, Experimental research on foil vibrations in a gas foil bearing carried out using an ultra-high-speed camera, Appl. Sci. 11 (2021) http://dx.doi.org/10.3390/app11020878, URL https://www.mdpi.com/2076-3417/11/2/878.

[11] A.M. Ahmed, M. Abdelrazek, S. Aryal, T.T. Nguyen, An overview of eulerian video motion magnification methods, Comput. Graph. 117 (2023) 145–163, http://dx.doi.org/10.1016/j.cag.2023.10.015, URL https://www.sciencedirect.com/science/article/pii/S0097849323002522.

[12] J. Zhong, S. Zhong, Q. Zhang, N. Maia, Y. Shen, S. Liu, Y. Yu, Z. Peng, Vision-based system for simultaneous monitoring of shaft rotational speed and axial vibration using non-projection composite fringe pattern, Mech. Syst. Signal Process. 120 (2019) 765–776, http://dx.doi.org/10.1016/j.ymssp.2018.11.006, URL https://www.sciencedirect.com/science/article/pii/S0888327018307258.

[13] H. André, Q. Leclère, D. Anastasio, Y. Benaïcha, K. Billon, M. Birem, F. Bonnardot, Z. Chin, F. Combet, P. Daems, A. Daga, R. De Geest, B. Elyousfi, J. Griffaton, K. Gryllias, Y. Hawwari, J. Helsen, F. Lacaze, L. Laroche, X. Li, C. Liu, A. Mauricio, A. Melot, A. Ompusunggu, G. Paillot, S. Passos, C. Peeters, M. Perez, J. Qi, E. Sierra-Alonso, W. Smith, X. Thomas, Using a smartphone camera to analyse rotating and vibrating systems: Feedback on the survishno 2019 contest, Mech. Syst. Signal Process. 154 (2021) 107553, http://dx.doi.org/10.1016/j.ymssp.2020.107553, URL https://www.sciencedirect.com/science/article/pii/S0888327020309390.

[14] Y. Wang, L. Wang, Y. Yan, Rotational speed measurement through digital imaging and image processing, in: 2017 IEEE International Instrumentation and Measurement Technology Conference, I2MTC, 2017, pp. 1–6, http://dx.doi.org/10.1109/I2MTC.2017.7969697.

[15] T. Wang, Y. Yan, L. Wang, Y. Hu, Rotational speed measurement through image similarity evaluation and spectral analysis, IEEE Access 6 (2018) 46718–46730, http://dx.doi.org/10.1109/ACCESS.2018.2866479.

[16] T. Verwimp, A. Mauricio, K. Gryllias, Rotating machinery speed extraction through smartphone video acquisition from a radial viewpoint, Mech. Syst. Signal Process. 205 (2023) 110836, http://dx.doi.org/10.1016/j.ymssp.2023.110836, URL https://www.sciencedirect.com/science/article/pii/S0888327023007446.

[17] Y. Zhao, Y. Li, S. Guo, T. Li, Measuring the angular velocity of a propeller with video camera using electronic rolling shutter, J. Sens. 2018 (2018) 1037083, http://dx.doi.org/10.1155/2018/1037083, URL https://onlinelibrary.wiley.com/doi/abs/10.1155/2018/1037083. arXiv:https://onlinelibrary.wiley.com/doi/pdf/10.1155/2018/1037083.

[18] X. Wang, J. Guo, S. Lu, C. Shen, Q. He, A computer-vision-based rotating speed estimation method for motor bearing fault diagnosis, Meas. Sci. Technol. 28 (2017) 065012, http://dx.doi.org/10.1088/1361-6501/aa650a.

[19] F. Natili, F. Castellani, D. Astolfi, M. Becchetti, Video-tachometer methodology for wind turbine rotor speed measurement, Sensors 20 (2020) http://dx.doi.org/10.3390/s20247314, URL https://www.mdpi.com/1424-8220/20/24/7314.

[20] H. Zhao, X. Zhang, D. Jiang, J. Gu, Research on rotating machinery fault diagnosis based on an improved eulerian video motion magnification, Sensors 23 (2023) http://dx.doi.org/10.3390/s23239582, URL https://www.mdpi.com/1424-8220/23/23/9582.

[21] C. Li, J. Zhou, X. Wu, T. Liu, Phase-based video vibration measurement and fault feature extraction method for compound faults of rolling bearings, Adv. Eng. Inform. 62 (2024) 102897, http://dx.doi.org/10.1016/j.aei.2024.102897, URL https://www.sciencedirect.com/science/article/pii/S1474034624005482.

[22] J. Antoni, J. Griffaton, H. André, L.D. Avendaño-Valencia, F. Bonnardot, O. Cardona-Morales, G. Castellanos-Dominguez, A.P. Daga, Q. Leclère, C.M. Vicuña, D.Q. Acuña, A.P. Ompusunggu, E.F. Sierra-Alonso, Feedback on the surveillance 8 challenge: Vibration-based diagnosis of a safran aircraft engine, Mech. Syst. Signal Process. 97 (2017) 112–144, http://dx.doi.org/10.1016/j.ymssp.2017.01.037, URL https://www.sciencedirect.com/science/article/pii/S0888327017300584. [special Issue on Surveillance].

[23] Q. Leclère, H. André, J. Antoni, A multi-order probabilistic approach for instantaneous angular speed tracking debriefing of the cmmno2014 diagnosis contest, Mech. Syst. Signal Process. 81 (2016) 375–386, http://dx.doi.org/10.1016/j.ymssp.2016.02.053, URL https://www.sciencedirect.com/science/article/pii/S0888327016001047.

[24] A. Marsick, H. André, I. Khelf, Q. Leclère, J. Antoni, Restoring cyclostationarity of rolling element bearing signals from the instantaneous phase of their envelope, Mech. Syst. Signal Process. 193 (2023) 110264, http://dx.doi.org/10.1016/j.ymssp.2023.110264, URL https://www.sciencedirect.com/science/article/pii/S0888327023001711.

[25] C. Zhang, Z. Meng, Y. Wang, Z. Yang, H. Jiang, B. Li, Fault signature extraction of rolling bearings under variable speed via time–frequency overlap group sparse representation, Mech. Syst. Signal Process. 223 (2025) 111823, http://dx.doi.org/10.1016/j.ymssp.2024.111823, URL https://www.sciencedirect.com/science/article/pii/S0888327024007210.

[26] A. Mauricio, W.A. Smith, R.B. Randall, J. Antoni, K. Gryllias, Improved envelope spectrum via feature optimisation-gram (iesfogram): A novel tool for rolling element bearing diagnostics under non-stationary operating conditions, Mech. Syst. Signal Process. 144 (2020) 106891, http://dx.doi.org/10.1016/j.ymssp.2020.106891, URL https://www.sciencedirect.com/science/article/pii/S0888327020302776.

[27] D. Abboud, Y. Marnissi, A. Assoumane, Y. Hawwari, M. Elbadaoui, Synchronous analysis of cyclo-non-stationary signals: A comprehensive study with aeronautic applications, Mech. Syst. Signal Process. 168 (2022) 108600, http://dx.doi.org/10.1016/j.ymssp.2021.108600, URL https://www.sciencedirect.com/science/article/pii/S0888327021009316.

[28] C. Peeters, Q. Leclère, J. Antoni, P. Lindahl, J. Donnal, S. Leeb, J. Helsen, Review and comparison of tacholess instantaneous speed estimation methods on experimental vibration data, Mech. Syst. Signal Process. 129 (2019) 407–436, http://dx.doi.org/10.1016/j.ymssp.2019.02.031, URL https://www.sciencedirect.com/science/article/pii/S0888327019301153.

[29] D. Peng, W.A. Smith, R.B. Randall, K. Feng, Z. Peng, W. Teng, Y. Liu, Iterative improvement in tacholess speed estimation using instantaneous error estimation for machine condition monitoring in variable speed, Mech. Syst. Signal Process. 216 (2024) 111488, http://dx.doi.org/10.1016/j.ymssp.2024.111488, URL https://www.sciencedirect.com/science/article/pii/S0888327024003868.

[30] F. Bonnardot, Influence of speed fluctuation on cepstrum, Mech. Syst. Signal Process. 119 (2019) 81–99, http://dx.doi.org/10.1016/j.ymssp.2018.09.010, URL https://www.sciencedirect.com/science/article/pii/S0888327018306204.

[31] W.A. Smith, P. Borghesani, R.B. Randall, J. Antoni, M. El Badaoui, Z. Peng, High-speed bearing diagnostics: Observations from the surveillance 8 safran contest data, Mech. Syst. Signal Process. 216 (2024) 111484, http://dx.doi.org/10.1016/j.ymssp.2024.111484, URL https://www.sciencedirect.com/science/article/pii/S0888327024003820.

[32] C. Yang, H. Li, S. Cao, K. Zhang, W. Xiang, A fast method for robust estimation of gearbox instantaneous speed, Mech. Syst. Signal Process. 212 (2024) 111273, http://dx.doi.org/10.1016/j.ymssp.2024.111273, URL https://www.sciencedirect.com/science/article/pii/S0888327024001717.

[33] D. Peng, Y. Chen, M.J. Zuo, C.K. Mechefske, Assessment and improvement of the accuracy of tacholess instantaneous speed estimation, Mech. Syst. Signal Process. 202 (2023) 110706, http://dx.doi.org/10.1016/j.ymssp.2023.110706, URL https://www.sciencedirect.com/science/article/pii/S0888327023006143.

[34] D. Peng, W.A. Smith, R.B. Randall, Z. Peng, C.K. Mechefske, Speed estimation in planetary gearboxes: A method for reducing impulsive noise, Mech. Syst. Signal Process. 159 (2021) 107786, http://dx.doi.org/10.1016/j.ymssp.2021.107786, URL https://www.sciencedirect.com/science/article/pii/S0888327021001813.

[35] C. Peeters, J. Antoni, Q. Leclère, T. Verstraeten, J. Helsen, Multi-harmonic phase demodulation method for instantaneous angular speed estimation using harmonic weighting, Mech. Syst. Signal Process. 167 (2022) 108533, http://dx.doi.org/10.1016/j.ymssp.2021.108533, URL https://www.sciencedirect.com/science/article/pii/S088832702100875X.

[36] Y. Li, C. Geng, M.J. Zuo, X. Liang, Use of vibration signal to estimate instantaneous angular frequency under strong nonstationary regimes, Mech. Syst. Signal Process. 200 (2023) 110571, http://dx.doi.org/10.1016/j.ymssp.2023.110571, URL https://www.sciencedirect.com/science/article/pii/S088832702300479X.

[37] D. Abboud, M. Elbadaoui, W. Smith, R. Randall, Advanced bearing diagnostics: A comparative study of two powerful approaches, Mech. Syst. Signal Process. 114 (2019) 604–627, http://dx.doi.org/10.1016/j.ymssp.2018.05.011, URL https://www.sciencedirect.com/science/article/pii/S0888327018302619.

[38] A.P. Daga, L. Garibaldi, C. He, J. Antoni, Key-phase-free blade tip-timing for nonstationary test conditions: An improved algorithm for the vibration monitoring of a safran turbomachine from the surveillance 9 international conference contest, Machines 9 (2021) http://dx.doi.org/10.3390/machines9100235, URL https://www.mdpi.com/2075-1702/9/10/235.

[39] A. Rivola, M. Troncossi, Zebra tape identification for the instantaneous angular speed computation and angular resampling of motorbike valve train measurements, Mech. Syst. Signal Process. 44 (2014) 5–13, http://dx.doi.org/10.1016/j.ymssp.2012.11.009, URL https://www.sciencedirect.com/science/article/pii/S0888327012004670. [special Issue on Instantaneous Angular Speed (IAS) Processing and Angular Applications].

[40] A.P. Daga, L. Garibaldi, Ga-adaptive template matching for offline shape motion tracking based on edge detection: Ias estimation from the survishno 2019 challenge video for machine diagnostics purposes, Algorithms 13 (2020) http://dx.doi.org/10.3390/a13020033, URL https://www.mdpi.com/1999-4893/13/2/33.

[41] G. Jocher, A. Chaurasia, A. Stoken, J. Borovec, NanoCode012, Y. Kwon, K. Michael, TaoXie, J. Fang, imyhxy, Lorna, Z. Yifu, C. Wong, A. V, D. Montes, Z. Wang, C. Fati, J. Nadar, Laughing, UnglvKitDe, V. Sonck, tkianai, O.N.G. yxN, P. Skalski, A. Hogan, D. Nair, M. Strobel, M. Jain, Ultralytics/yolov5: v7.0 - YOLOv5 SOTA realtime instance segmentation, 2022, http://dx.doi.org/10.5281/zenodo.7347926.

[42] J.Y. Bouguet, Pyramidal Implementation of the Affine Lucas Kanade Feature Tracker Description of the Algorithm, Technical Report, Intel Corporation, Microprocessor Research Labs, 2000.

[43] R.B. Randall, J. Antoni, Rolling element bearing diagnostics—a tutorial, Mech. Syst. Signal Process. 25 (2011) 485–520, http://dx.doi.org/10.1016/j.ymssp.2010.07.017, URL https://www.sciencedirect.com/science/article/pii/S0888327010002530.

[44] A. Marsick, J. Touzet, A. Burel, Q. Leclère, H. André, d. Remond, Survishno 2023 contest data files, 2024, http://dx.doi.org/10.5281/zenodo.13707571.